AD-A172 113 ULTRASONIC SCATTERING BY PLANAR AND NON-PLANAR CRACKS (U) COLORADO UNIV AT BOULDER DEPT OF MECHANICAL ENGINEERING S K DATTA ET AL. AUG 86 CUMER-86-4 1/1

UNCLASSIFIED N00014-86-K-0280 F/G 20/11 NL

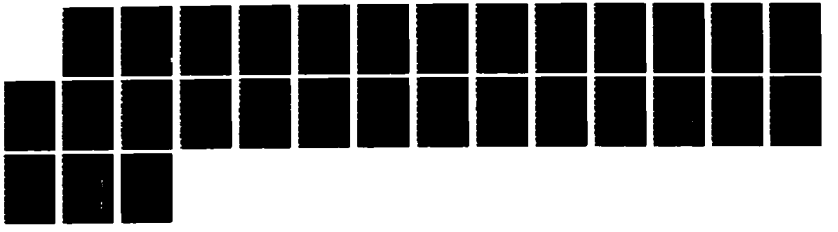

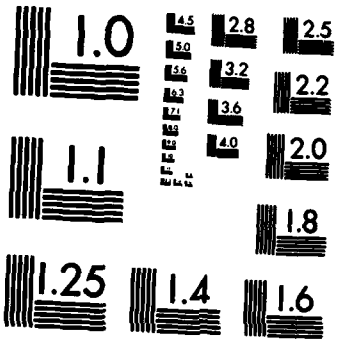

ULATRASONIC SCATTERING BY PLANAR AND NON-PLANAR CRACKS

Subhendu K. Datta[1]

Arvind H. Shah[2]

CUMER-86-4 August 1986

Contract N00014-86-K-0280

[1]Department of Mechanical Engineering and
Cooperative Institute for Research in Environmental Sciences
University of Colorado
Boulder, CO 80309, U.S.A.

[2]Department of Civil Engineering
University of Manitoba
Winnipeg, Canada R3T 2N2

Elastic Wave Scattering by Surface-Breaking Planar and Non-Planar Cracks

A. H. Shah and Y. F. Chin
Department of Civil Engineering
University of Manitoba, Winnipeg

S. K. Datta
Department of Mechanical Engineering and CIRES
University of Colorado, Boulder
Fellow, ASME

Abstract

Scattering of elastic waves by surface-breaking planar and non-planar (branched) cracks has been studied in this paper. Attention has been focused on the near-field surface displacements and the crack-tip(s) stress-intensity factors. For planar normal cracks the stress-intensity factors are shown to agree with earlier results. Numerical results showing normalized vertical surface displacements are presented for incident body and surface waves. It is shown that the results for planar and branched cracks can be significantly different in some instances.

Introduction

Problems of elastic wave scattering by surface-breaking and near-surface cracks are of considerable current interest for ultrasonic nondestructive evaluation. Ultrasonic scattering by planar cracks near or at the free surface of a semi-infinite elastic homogeneous medium has been studied theoretically by many authors. References to recent papers on this subject can be found in [1], [2] and [3]. Some experimental works on surface-breaking normal planar cracks have also appeared ([4-6]).

Ultrasonic scattering by surface-breaking planar and branched cracks of arbitrary orientation is the subject of this investigation. To our knowledge this problem has not received much attention in the literature. An approximate solution that is valid at low frequencies was

presented in [7] for SH wave diffraction by a canted surface-breaking planar crack. Subsequently, a hybrid finite element and eigenfunction technique was used in [8] to study SH wave diffraction by planar surface-breaking canted crack.

In this paper we use the same hybrid technique as in [8] to study the scattering of in-plane body and surface waves by canted planar and normal surface-breaking branched cracks. We focus our attention to the near-field. Numerical results are presented for the vertical surface displacement amplitudes near the base of the crack and crack-tip(s) stress-intensity factors.

Formulation and Solution

Consider a homogeneous, isotropic, and linearly elastic medium with a surface-breaking crack of arbitrary orientation and shape as shown in Figure 1. Assume the displacement $\underset{\sim}{u}(x,y,t)$ at a point P to be time-harmonic of the form $\underset{\sim}{u}(x,y)e^{-i\omega t}$ where ω is the circular frequency. Then $\underset{\sim}{u}$ satisfies the equation of motion in $y > 0$ (at points not on the crack)

$$\mu\nabla^2\underset{\sim}{u} + (\lambda + \mu)\,\underset{\sim}{\nabla}\underset{\sim}{\nabla}\cdot\underset{\sim}{u} = -\rho\omega^2\underset{\sim}{u} \tag{1}$$

where λ, μ are Lamé constants, ρ the mass density and the factor $e^{-i\omega t}$ has been dropped.

The solution of (1) can be expressed in terms of longitudinal and shear wave potentials, ϕ and ψ, in the form

$$\underset{\sim}{u} = \underset{\sim}{\nabla}\phi + \underset{\sim}{\nabla}\times(\psi\underset{\sim}{e}_z) \tag{2}$$

Furthermore, in a homogeneous half-space, ϕ and ψ can be expressed in infinite series of multipolar potentials as [9].

$$\begin{aligned}\phi &= \sum_{n=-\infty}^{\infty}\left(a_n\phi_n^p + b_n\phi_n^s\right)\\ \psi &= \sum_{n=-\infty}^{\infty}\left(a_n\psi_n^p + b_n\psi_n^s\right)\end{aligned} \tag{3}$$

where expressions for ϕ_n^p, ψ_n^p, ϕ_n^s and ψ_n^s, can be found in [9]. The coefficients a_n, b_n are found by satisfying the appropriate boundary conditions.

The representation (3) is not useful for satisfying the boundary conditions on the crack surface. For this reason, a different representation is needed in this near-field region. In this paper, the region inside the fictitious boundary B (Fig. 1) is divided into finite elements having N_I number of interior nodes and N_B number of boundary nodes.

For the finite element representation in region II, the energy functional is taken to be

$$F = \frac{1}{2}\int\int_{R_{II}} \left(\underline{\sigma}\cdot\underline{\epsilon}^* - \rho\omega^2 \underline{u}\cdot\underline{u}^*\right) dxdy$$

$$- \frac{1}{2}\int_B \left(\underline{P}_B\cdot\underline{u}_B^* + \underline{P}_B^*\cdot\underline{u}_B\right) ds \tag{4}$$

where '$*$' indicates complex conjugate and $\underline{\sigma}$ and $\underline{\epsilon}$ are column vectors defined as

$$\underline{\sigma} = \{\sigma\} = \left(\sigma_{xx}, \sigma_{yy}, \sigma_{xy}\right)^T \tag{5}$$

$$\underline{\epsilon} = \{\epsilon\} = \left(\epsilon_{xx}, \epsilon_{yy}, \epsilon_{xy}\right)^T \tag{6}$$

Superscript 'T' denotes transpose. The $\underline{P}_B$ and $\underline{U}_B$ represent the traction and displacement on B, respectively.

It is assumed that the displacement field within the j^{th} element is represented in terms of the shape functions $L_j(x, y)$ and elemental nodal displacements $\{\underline{q}_j^e\}$ as

$$\underline{u}^e = \sum_{j=1}^{N_e} L_j \underline{q}_j^e \tag{7}$$

where each $\underline{q}_j^e$ has two components u_{xj} and u_{yj} along the x and y directions, respectively. The N_e represents the number of nodes in each element.

The σ_{ij}^{e} and ϵ_{ij}^{e} are computed by substituting Eq. (7) into strain-displacement relations and these, in turn, into the stress-strain relations. Using these in Eq. (4), we get

$$F = \underset{\sim}{q}_I^{*T} S_{II}\, \underset{\sim}{q}_I + \underset{\sim}{q}_I^{*T} S_{IB}\, \underset{\sim}{q}_B + \underset{\sim}{q}_B^{*T} S_{BI}\, \underset{\sim}{q}_I + \underset{\sim}{q}_B^{*T} S_{BB}\, \underset{\sim}{q}_B - \underset{\sim}{q}^{*T} P_B^{(1)} - \underset{\sim}{P}_B^{*T(1)}\, \underset{\sim}{q}_B \tag{8}$$

in which $\underset{\sim}{q}_I = \underset{\sim}{q}_I^{(2)}$, $\underset{\sim}{q}_B = \underset{\sim}{q}_B^{(2)}$, $\underset{\sim}{P}_B^{(1)} = \underset{\sim}{P}_B^{(2)}$ and the elemental impedance matrices S_{ij} are defined as

$$\left[S^e\right] = \int\int_{R_e} \left([B^e]^T [D][B^e] - \rho_e \omega^2 [L]^T [L] \right) dxdy \ . \tag{9}$$

In Eq. (9),

$$[B^e] = \begin{bmatrix} \dfrac{\partial}{\partial x} & 0 \\ 0 & \dfrac{\partial}{\partial y} \\ \dfrac{\partial}{\partial y} & \dfrac{\partial}{\partial x} \end{bmatrix} \begin{bmatrix} L_1 & 0 & L_2 & .. \\ 0 & L_1 & 0 & .. \end{bmatrix} = [N][L] \ .$$

Note that [L] is a $2 \times 2N_e$ matrix.

For an isotropic material [D] is given by

$$[D] = \begin{bmatrix} \lambda_e + 2\mu_e & \lambda_e & 0 \\ \lambda_e & \lambda_e + 2\mu_e & 0 \\ 0 & 0 & \mu_e \end{bmatrix}$$

where λ_e and μ_3 are the Lame's constant.

To find the constants a_n, b_n appearing in (3) and the nodal displacements in region II, it is necessary to use the continuity of displacement and traction on B. This is discussed in the following.

The incident displacement fields will be assumed to arise from the incident plane P and SV waves, and their reflections from the free surface $y = 0$. The case of incident Rayleigh waves will also be considered.

Let us suppose that in the absence of the crack the free field is the sum of the incident and reflected fields, that is

$$u_j^{(0)} = u_j^{(i)} + u_j^{(r)} \qquad (j = 1,2) \ . \tag{10}$$

For the Rayleigh wave $u_j^{(0)}$ is the associated displacement.

The total field outside B then is

$$u_j = u_j^{(s)} + u_j^{(0)} \qquad (j = 1,2) \tag{11}$$

where $u_j^{(s)}$ is given by (2) and (3).

Using (2) and (3), the displacements at the nodes on B can be written as

$$\{\underline{q}_B^{(s)}\} = [G]\{\underline{a}\} \tag{12}$$

where $[G]$ is a $2N_B \times 2N_B$ matrix formulated in Appendix A and vector $\{\underline{a}\}$ is

$$\{\underline{a}\} = \left[a_1, \cdots, a_{N_B}, b_1, \cdots, b_{N_B}\right]^T$$

Similarly, using (2) and (3) in the stress strain relation, the traction at the nodes on B can be expressed in the form

$$\{\underline{\sigma}_B^{(s)}\} = [F]\{\underline{a}\} \tag{13}$$

where $[F]$ is also a $2N_B \times 2N_B$ matrix defined in Appendix A.

To express $\{\underline{\sigma}_B^{(s)}\}$ in terms of $\{\underline{q}_B^{(s)}\}$, we use the expression for the virtual work done on the boundary B, which is

$$\delta\pi = \int_B \{\delta \underline{q}_B^{*(1)}\}^T \{\underline{\sigma}_B^{(1)}\} d\Gamma \tag{14}$$

where superscript (1) denotes the total field in region I (outside B).

Because of the continuity of displacements and traction on B, we have

$$\underline{q}_B^{(1)} = \underline{q}_B^{(2)} = \underline{q}_B^{(0)} + \underline{q}_B^{(s)} \tag{15}$$

$$\underline{\sigma}_B^{(1)} = \underline{\sigma}_B^{(2)} = \underline{\sigma}_B^{(0)} + \underline{\sigma}_B^{(s)} \tag{16}$$

where superscript (2) denotes the total field in region II.

Substituting (12), (13), (15), and (16) in Eqn. (14), and noting that $\delta \underline{q}_B^{(1)} = \delta \underline{q}_B^{(s)}$, we obtain from Eqn. (14)

$$\delta\pi = \{\delta \underline{a}^*\}^T \{\underline{P}_B^{(1)}\} \tag{17}$$

where $\underline{P}_B^{(1)}$ is given by

$$\{\underline{P}_B^{(1)}\} = [\overline{R}]\{\underline{a}\} + \{\underline{P}_B^{(0)}\} \tag{18}$$

Here

$$[\overline{R}] = \int_B [G^*]^T [F] d\Gamma \tag{19}$$

and

$$\{\underline{P}_B^{(0)}\} = \int_B [G^*]^T \{\underline{\sigma}_B^{(0)}\} d\Gamma \tag{20}$$

Equations (19) and (20) are approximated by

$$[\overline{R}] = [G^*]^T [F] * R\,\Delta\theta \tag{21}$$

and

$$\{\underline{P}_B^{(0)}\} = [G^*]^T \{\underline{\sigma}_B^{(0)}\} * R\,\Delta\theta \tag{22}$$

where $R\,\Delta\theta$ is the arc length between two adjacent boundary nodes on contour B. Note that the first two rows and last two rows of Eqs. (21) and (22) are multiplied by $R\,\frac{\Delta\theta}{2}$ instead of

$R\,\Delta\theta$, because they correspond to the first and last boundary nodes, respectively.

Substituting Eqn. (12) in Eqn. (8) and taking the variation, we obtain a set of simultaneous equations which may be written in matrix form as

$$\begin{bmatrix} S_{II} & S_{IB}\,G_I \\ G^{*T} S_{IB}^T & G^{*T} S_{BB}\,G \end{bmatrix} \begin{bmatrix} \underline{q}_I \\ \underline{a} \end{bmatrix} = \begin{bmatrix} -S_{IB}\,\underline{q}_B^{(0)} \\ -G^{*T} S_{BB}\,\underline{q}_B^{(0)} + \underline{P}_B^{(1)} \end{bmatrix} . \tag{23}$$

The first equation of Eqn. (23) can be written as:

$$\underline{q}_I = -\,S_{II}^{-1}\left[S_{IB}\,G\underline{a} + S_{IB}\,\underline{q}_B^{(0)}\right] . \tag{24}$$

The second equation can be written as

$$G^{*T} S_{IB}^T\,\underline{q}_I + G^{*T} S_{BB}\,G\,\underline{a} = -\,G^{*T} S_{BB}\,\underline{q}_B^{(0)} + \underline{P}_B^{(1)} . \tag{25}$$

Substituting Eqs. (18) and (24) into Eq. (25), we obtain

$$\begin{aligned} &\left[G^{*T}\left(S_{BB} - S_{IB}^T S_{II}^{-1} S_{IB}\right) G^* - \bar{R}\right]\{\underline{a}\} = \\ &\qquad -\,G^{*T}\left(S_{BB} - S_{IB}^T S_{II}^{-1} S_{IB}\right)\underline{q}_B^{(0)} + \underline{P}_B^{(0)} \end{aligned} \tag{26}$$

In Eq. (26), the generalized coordinates $\{\underline{a}\}$ are the only unknowns. Therefore, $\{\underline{a}\}$ can be evaluated. Once $\{\underline{a}\}$ are known, the near and far displacement and stress fields can be determined.

Numerical Results and Discussion

In this paper, the boundary B enclosing the interior region is not a complete circle, and so the potentials ϕ_n^p, ψ_n^p, and ϕ_n^s, ψ_n^s cannot be expanded in cylindrical wave functions as was done in [1]. So the integrals giving these potentials and their derivatives were evaluated numerically for every node on B. The details are discussed in [10].

The hybrid method is employed to study scattering by P, SV, and Rayleigh waves by

three types of surface breaking cracks: a vertical crack (Fig. 2 with $\alpha = 90°$), a 45° inclined crack (Fig. 2, with $\alpha = 45°$), and a vertical branched (Y) crack (Fig. 3). The Poisson's ratio of the material is taken to be 1/3.

Stress intensity factors at the tips of the cracks were calculated and for the particular case of a planar surface-breaking normal crack they were found to agree well with the results of [1]. These are shown in Figure 4.

Next, normalized stress-intensity factors are shown in Figures 5-7 for incident P, SV, and Rayleigh waves. It is seen that for P and Rayleigh waves the stress-intensity factors at the crack-tips of the three types of cracks are quite different, particularly at high frequencies. This is particularly significant for the branched crack, even though the branches are quite small.

The surface displacements at $y = 0$ are calculated by using (3) in (2) after $\{\tilde{a}\}$ are calculated. Normalized values of $u_y^{(s)}$ are presented in Figures 8-12. For each type of crack mentioned above five cases of incident waves were considered: plane P wave incident at 0° and 45°, plane SV wave incident at 0° and 45°, and finally Rayleigh wave. Some representative results are shown here.

Figures 8 and 9 show the scattered vertical surface displacement amplitudes for a Rayleigh wave incident from the left on a normal planar and branched crack. It is seen that there are large differences in the forward direction between the two cases as the frequency becomes large. In the backward direction, however, the differences are not very significant. Figures 10 and 11 show the results for an incident SV wave moving vertically as well as at 45° to the vertical. Large differences are found for vertical incidence, but not in the other case. Finally, in Figure 12 is shown the case of a Rayleigh wave incident on a canted crack. This figure is to be contrasted with Fig. 8. The large contrast shown clearly distinguishes a canted crack from a normal crack.

Conclusion

Model calculations of elastic wave scattering by surface-breaking planar and non-planar cracks have been presented. These calculations show that near-field surface displacements due to scattering by planar and branched cracks are quite different even when the branches are small. Also, it is found that signatures of normal and canted cracks are very dissimilar. These characteristic differences can be used to discriminate between the various cases.

Although the results presented here are for homogeneous medium, the technique can be generalized to study cracks in a composite medium. These are presently under investigation and will be reported later.

ACKNOWLEDGMENT

Results presented here were partly supported by grants from the Office of Naval Research (N00014-86-K-0280), the National Science Foundation (CEE81-20536) and the Natural Science and Engineering Research Council of Canada (A-7988).

References

1. Shah, A.H., Wong, K.C., and Datta, S.K., "Surface Displacements due to Elastic Wave Scattering by Planar and Non-Planar Cracks", *Wave Motion*, vol. 7, 1985, pp. 319-333.

2. Achenbach, J.D., Angel, Y.C., and Lin, W., "Scattering from Surface-Breaking and Near-Surface Cracks", in *Wave Propagation in Homogeneous Media and Ultrasonic Nondestructive Evaluation*, Johnson, G.C., ed., AMD-vol. 62, ASME, New York, 1984, pp. 93-109.

3. van der Hijden, J.H.M.T. and Neerhoff, F.L., "Diffraction of Elastic Waves by a Sub-Surface Crack (in-Plane Motion)", *Journal of the Acoustical Society of America*, vol. 75, 1984, pp. 1694-1704.

4. Hirao, M., Fukuoka, H., and Miura, Y., "Scattering of Rayleigh Surface Waves by Edge Cracks: Numerical Simulation and Experiment", *Journal of the Acoustical Society of America*, vol. 72, 1982, pp. 602-606.

5. Yew, C.H., Chen, K.G., and Wang, D.L., "An Experimental Study of Interaction between Surface Waves and a Surface Breaking Crack", *Journal of the Acoustical Society of America*, vol. 75, 1984, pp. 189-196.

6. Dong, R. and Adler, L., "Measurements of Reflection and Transmission Coefficients of Rayleigh Waves from Cracks", *Journal of the Acoustical Society of America*, vol. 76, 1984. pp. 1761-1763.

7. Datta, S.K., "Diffraction of SH-Waves by Edge Cracks", *ASME Journal of Applied Mechanics*, vol. 46, 1979, pp. 101-106.

8. Datta, S.K., Shah, A.H., and Fortunko, C.M., "Diffraction of Medium and Long Wavelength Horizontally Polarized Shear Waves by Edge Cracks", *Journal of Applied Physics*, vol. 53, 1982, pp. 2895-2903.

9. Datta, S.K. and El-Akily, N., "Diffraction of Elastic Waves by Cylindrical Cavity in a

Half-Space", *Journal of the Acoustical Society of America*, vol. 64, 1978, pp. 1692-1699.

10. Chin, Y.F., *Scattering of Elastic Waves by Near-Surface Inhomogeneities*, M.S. Thesis, University of Manitoba, 1985.

11. Achenbach, J.D., Keer, L.M., and Mendelsohn, D.A., "Elastodynamic Analysis of an Edge Crack", *ASME Journal of Applied Mechanics*, vol. 47, 1980, pp. 551-556.

APPENDIX A

Formulation of Matrices [G] and [F]

As mentioned before, the scattered nodal displacement vector, $\{\underline{q}_B^{(s)}\}$, was formed by evaluating $u_x^{(s)}$ and $u_y^{(s)}$ at N_B number of points on contour B. Thus, we have:

$$\{\underline{q}_B^{(s)}\} = [G]\,\{\underline{a}\} \tag{A-1}$$

where,

$$\{\underline{q}_B^{(s)}\} = \left\{u_{xB_1}, \cdots, u_{xB_{N_B}}, u_{yB_1}, \cdots, u_{yB_{N_B}}\right\}^T \tag{A-2}$$

$$\{\underline{a}\} = \{a_1, \cdots, a_{N_B}, b_1, \cdots, b_{N_B}\}^T \tag{A-3}$$

If [C] is partitioned as,

$$\left[\begin{array}{c|c} GXA & GXB \\ \hline GYA & GYB \end{array}\right]_{2N_B \times 2N_B} \tag{A-4}$$

then each of the $N_B \times N_B$ submatrix can be evaluated from Eqns. (2) and (3) at (x_i, y_i) on B as

$$\begin{aligned} (GXA)_{in} &= \left(\phi^P_{n,x} + \psi^P_{n,y}\right) \\ (GXB)_{in} &= \left(\phi^S_{n,x} + \psi^S_{n,y}\right) \\ (GYA)_{in} &= \left(\phi^P_{n,y} - \psi^P_{n,x}\right) \\ (GYB)_{in} &= \left(\phi^S_{n,y} - \psi^S_{n,x}\right) \quad , \; i = 1 \text{ to } N_B \end{aligned} \tag{A-5}$$

The parameter n in the summation series of Eqn. (3) is taken from $(-N_B/2 - 1)$ to $N_B/2$ for numerical purposes. Hence, n in the first column to the last column of each submatrix corresponds to $(-N_B/2 - 1)$ to $N_B/2$, respectively.

To formulate the matrix $[F]$, the components T_x and T_y of the traction vector T were calculated at each nodal point on B. If the radius vector of that point makes an angle β with the x-axes, then

$$T_x = \sigma_{xx}\cos\theta + \sigma_{xy}\sin\theta$$

$$T_y = \sigma_{xy}\cos\theta + \sigma_{yy}\sin\theta \quad . \tag{A-6}$$

Evaluating $\sigma_{xx}^{(s)}$, $\sigma_{yy}^{(s)}$, and $\sigma_{xy}^{(s)}$ at N_B number of points on contour B and substituting in Eqn. (A-6), we have the scattered nodal stress vector, $\{\underset{\sim}{\sigma}_B^{(s)}\}$, as in Eqn. (13),

$$\{\underset{\sim}{\sigma}_B^{(s)}\} = [F]\{\underset{\sim}{a}\} \tag{A-7}$$

where

$$\{\sigma_B^{(s)}\} = \left\{T_{xB_1}, \cdots, T_{yB_{N_B}}, \cdots, T_{yB_1}, \cdots, T_{yB_{N_B}}\right\} \tag{A-8}$$

and $\{\underset{\sim}{a}\}$ is defined in Eqn. (A-3)

$[F]$ is partitioned as

$$\left[\begin{array}{c|c} FXA & FYAB \\ \hline & \\ FYA & FYB \end{array}\right]_{2NB \times 2NB}$$

Each of the $N_B \times N_B$ submatrix can be evaluated at (x_i, y_i) on B as,

$$(FXA)_{in} = \left[(\lambda + 2\mu)(\phi^P_{n,xx} + \psi^P_{n,xy}) + \lambda(\phi^P_{n,yy} - \psi^P_{n,xy})\right]\cos\beta$$

$$+ \mu(2\phi^P_{n,xy} + \psi^P_{n,yy} - \psi^P_{n,xx})\sin\beta$$

$$(FXB)_{in} = \left[(\lambda - 2\mu)(\phi^{S}_{n,xz} - \psi^{S}_{n,zz} - \phi^{S}_{n,yy} - \psi^{S}_{n,xy})\right] \cos\beta$$

$$- \mu(2\phi^{S}_{n,xy} - \psi^{S}_{n,yy} - \psi^{S}_{n,xx}) \sin\beta$$

$$(FYA)_{in} = \mu(2\phi^{P}_{n,xy} - \psi^{P}_{n,yy} - \psi^{P}_{n,xx}) \cos\beta -$$

$$\left[(\lambda + 2\mu)(\phi^{P}_{n,yy} - \psi^{P}_{n,xy}) - \lambda(\phi^{P}_{n,xx} - \psi^{P}_{n,xy})\right] \sin\beta$$

$$(FYB)_{in} = \mu(2\phi^{S}_{n,xy} - \psi^{S}_{n,yy} - \psi^{S}_{n,xx}) \cos\beta -$$

$$\left[(\lambda + 2\mu)(\phi^{S}_{n,yy} - \psi^{S}_{n,xy}) + \lambda(\phi^{S}_{n,xx} + \psi^{S}_{n,xy})\right] \sin\beta$$

Parameter n ranges from $-(N_B/2 - 1)$ to $N_B/2$ as discused before, and $i = 1$ to N_B.

List of Figures

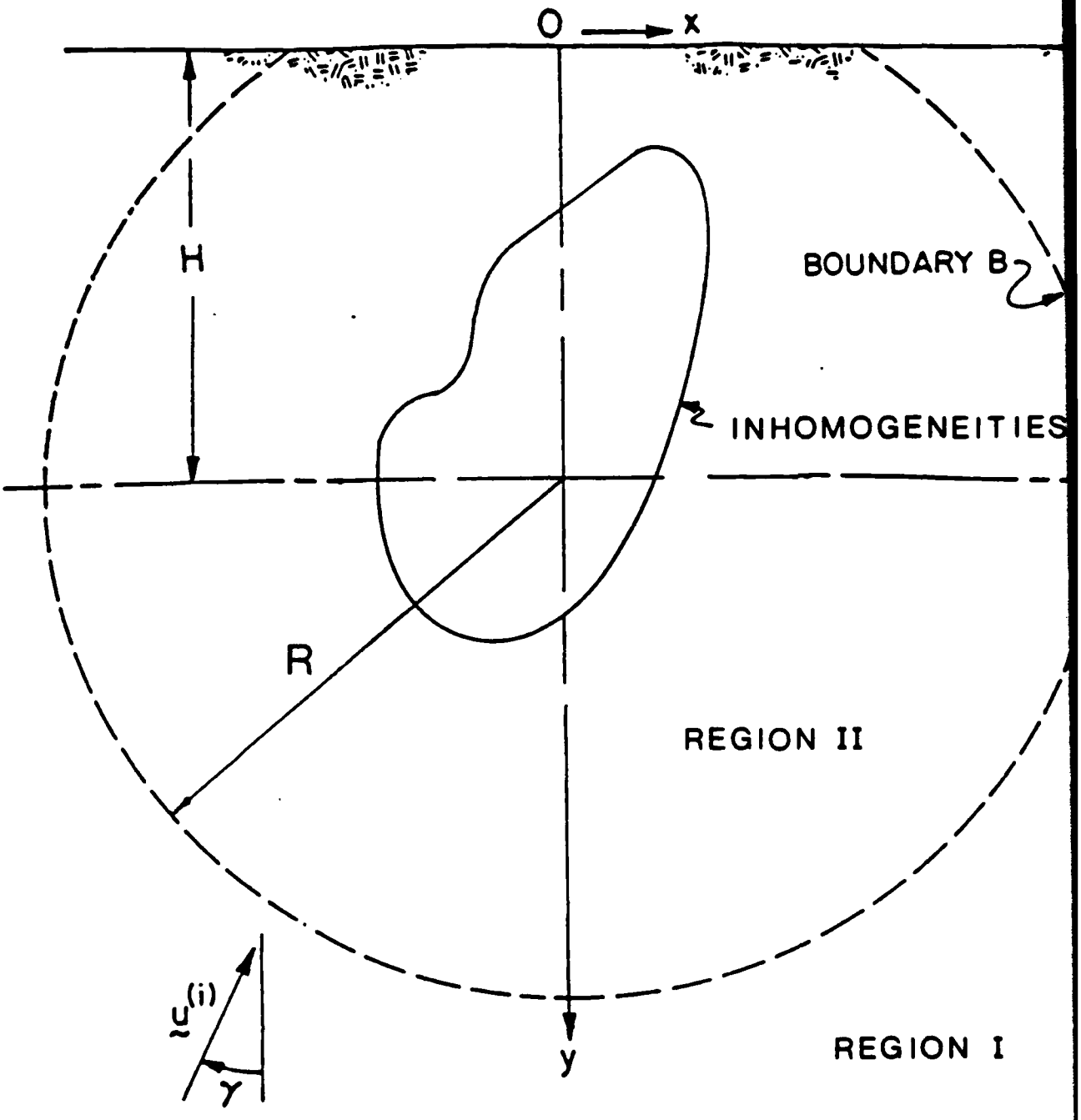
O
x
H
BOUNDARY B
INHOMOGENEITIES
R
REGION II
REGION I
y
$\underset{\sim}{u}^{(i)}$
γ

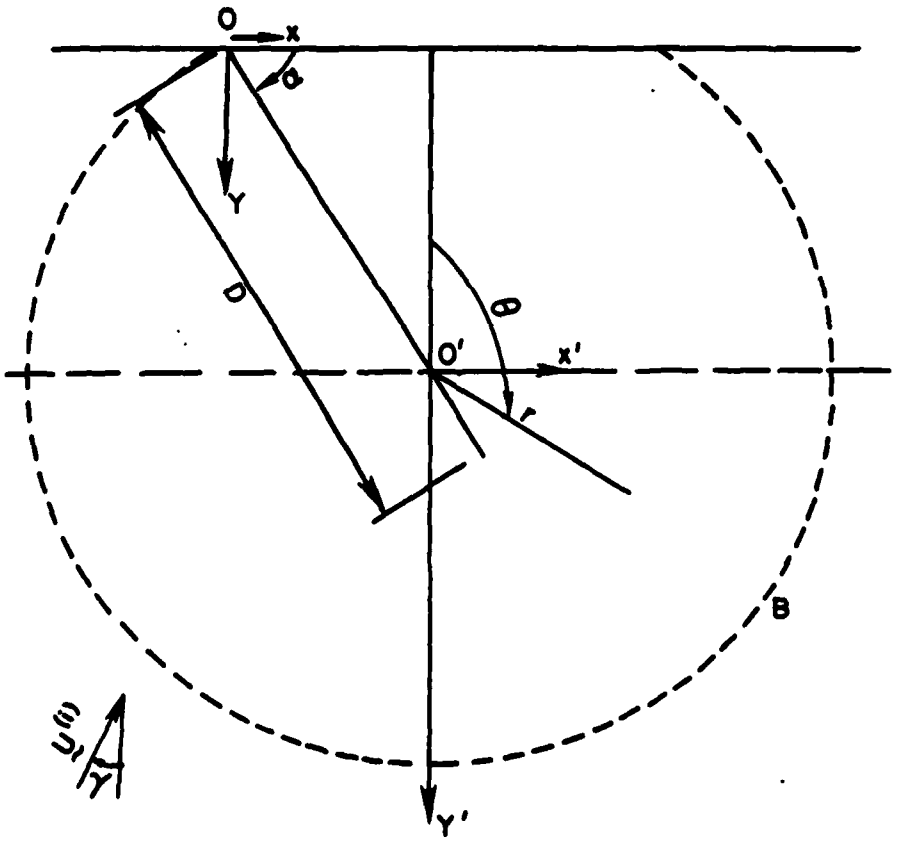
O
x
α
Y
D
θ
O'
x'
r
B
Y'

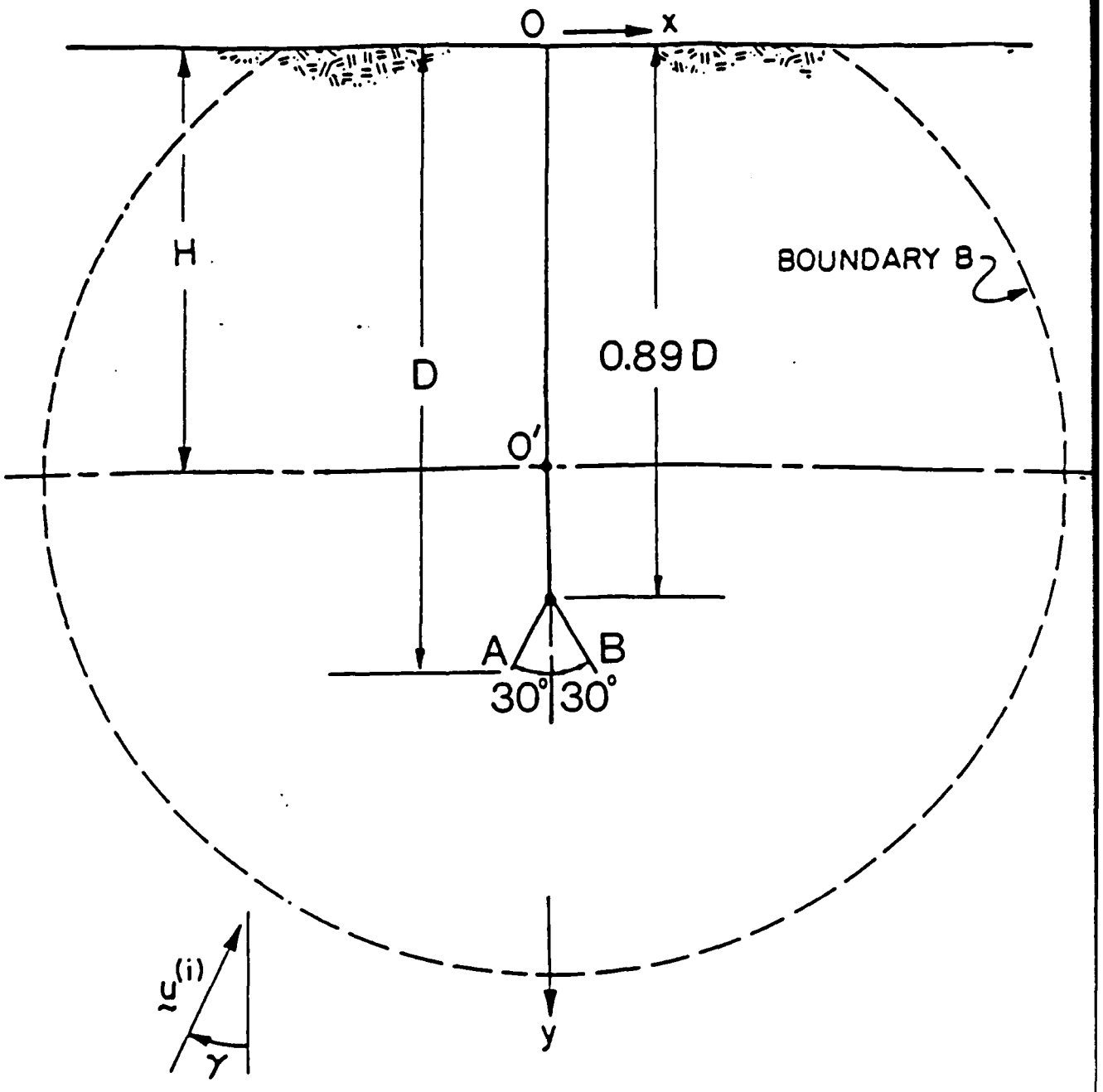
O
x
H
D
0.89D
BOUNDARY B
O'
A
B
30°
30°
y
γ

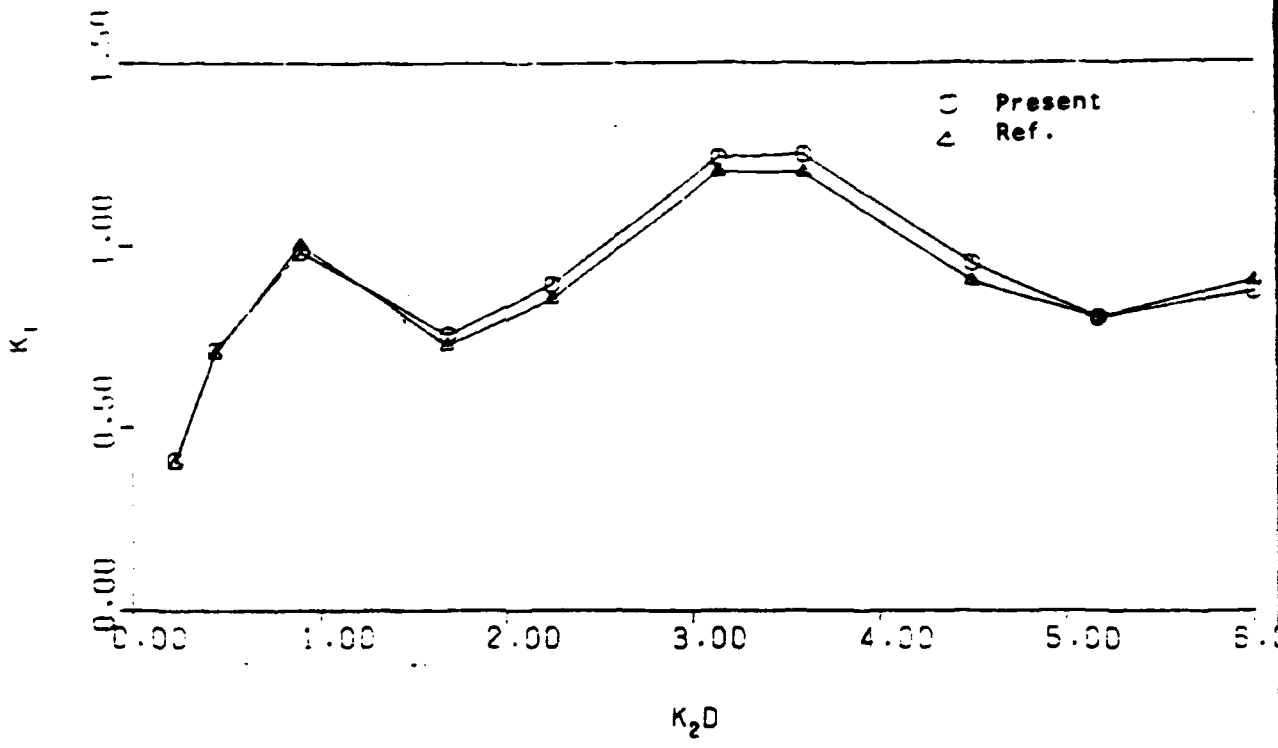
Present
Ref.
K_I
0.00
1.00
2.00
3.00
4.00
5.00
K_2D

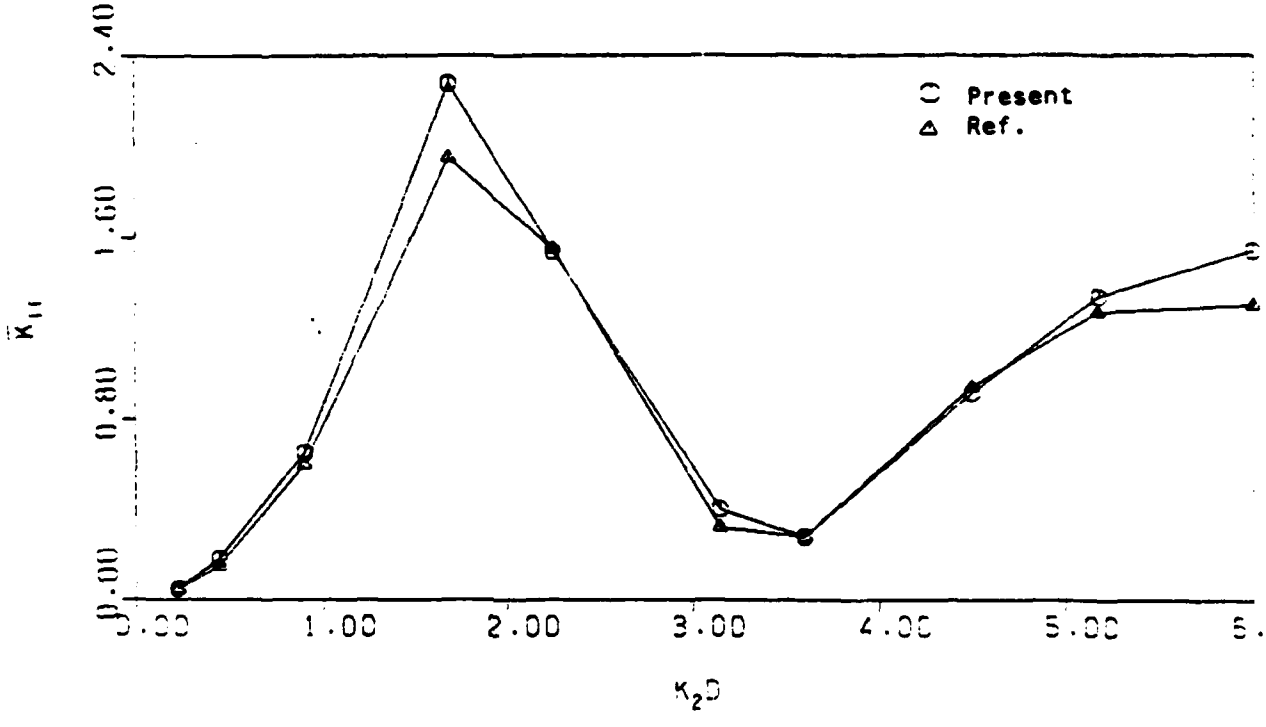
Present
Ref.
K_{II}
0.00
0.80
1.60
2.40
1.00
2.00
3.00
4.00
5.00
K_2D

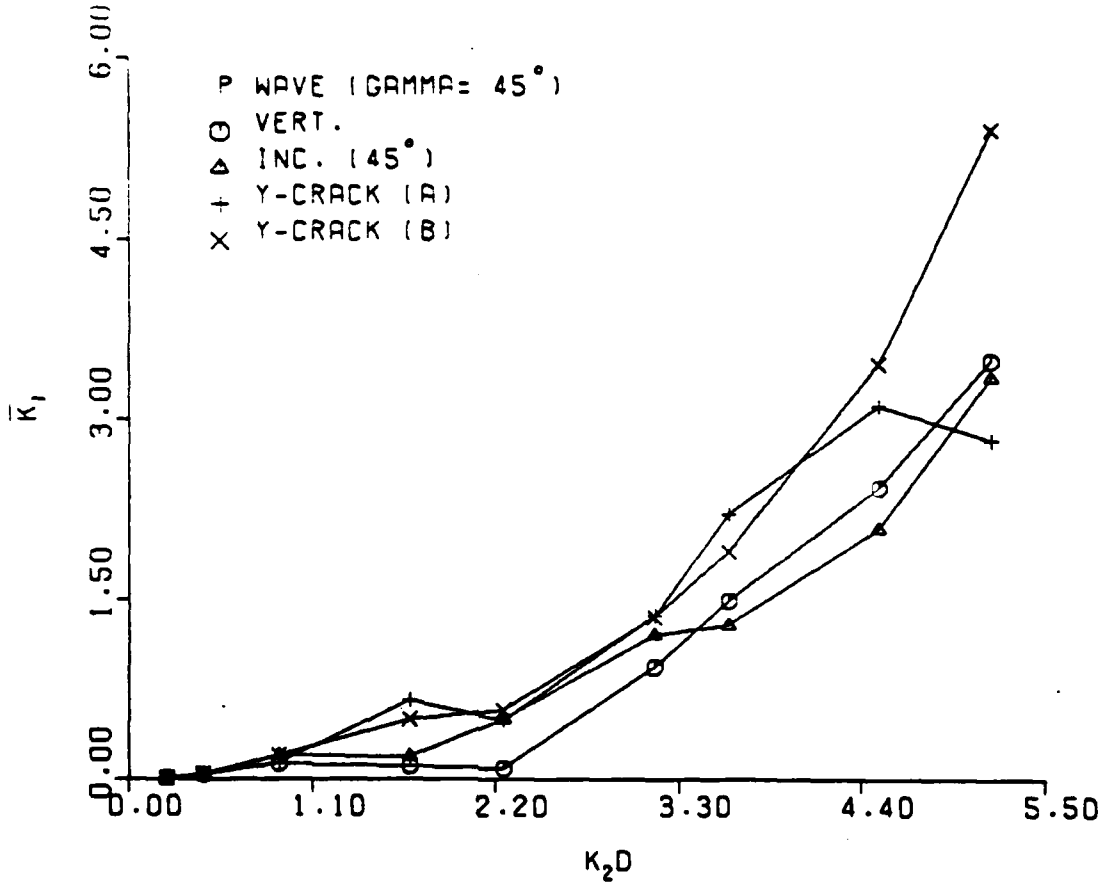
P WAVE (GAMMA= 45°)
VERT.
INC. (45°)
Y-CRACK (A)
Y-CRACK (B)
$\bar{K}_I$
6.00
4.50
3.00
1.50
0.00
0.00
1.10
2.20
3.30
4.40
5.50
K_2D

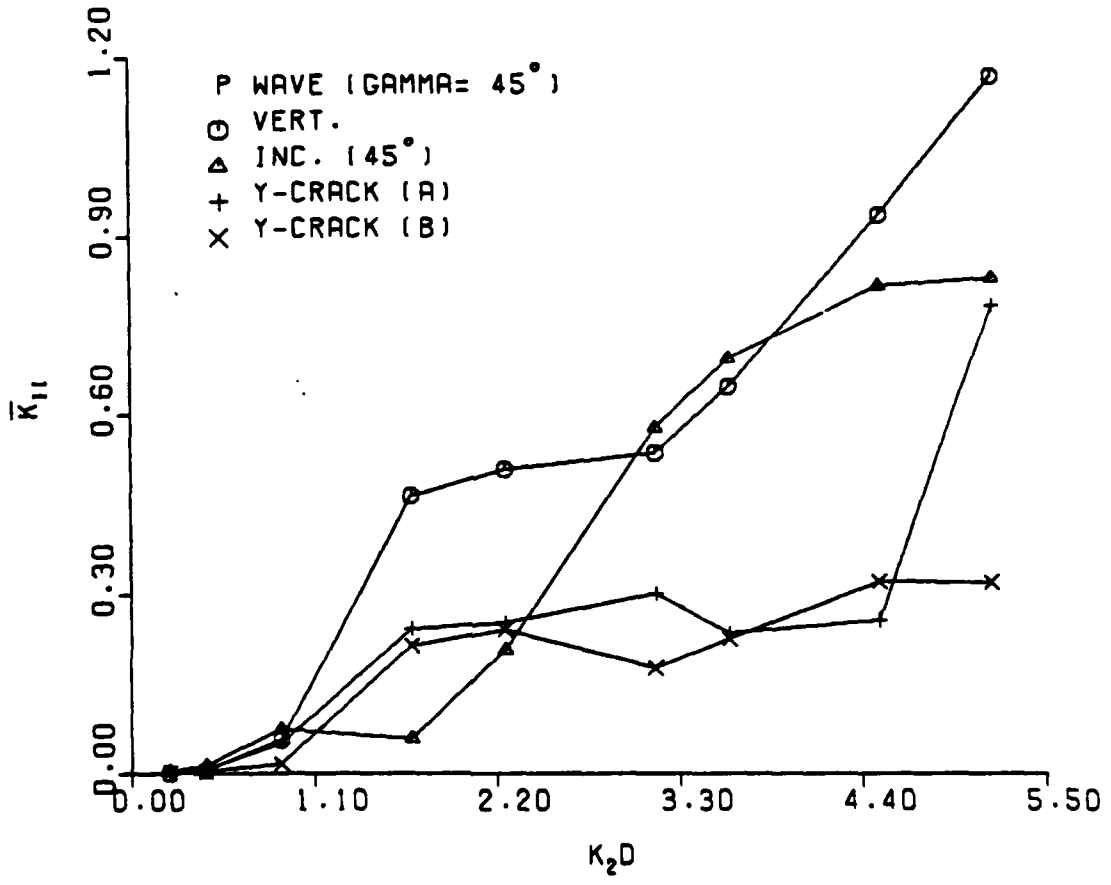
P WAVE (GAMMA= 45°)
VERT.
INC. (45°)
Y-CRACK (A)
Y-CRACK (B)
$\bar{K}_{II}$
1.20
0.90
0.60
0.30
0.00
0.00
1.10
2.20
3.30
4.40
5.50
K_2D

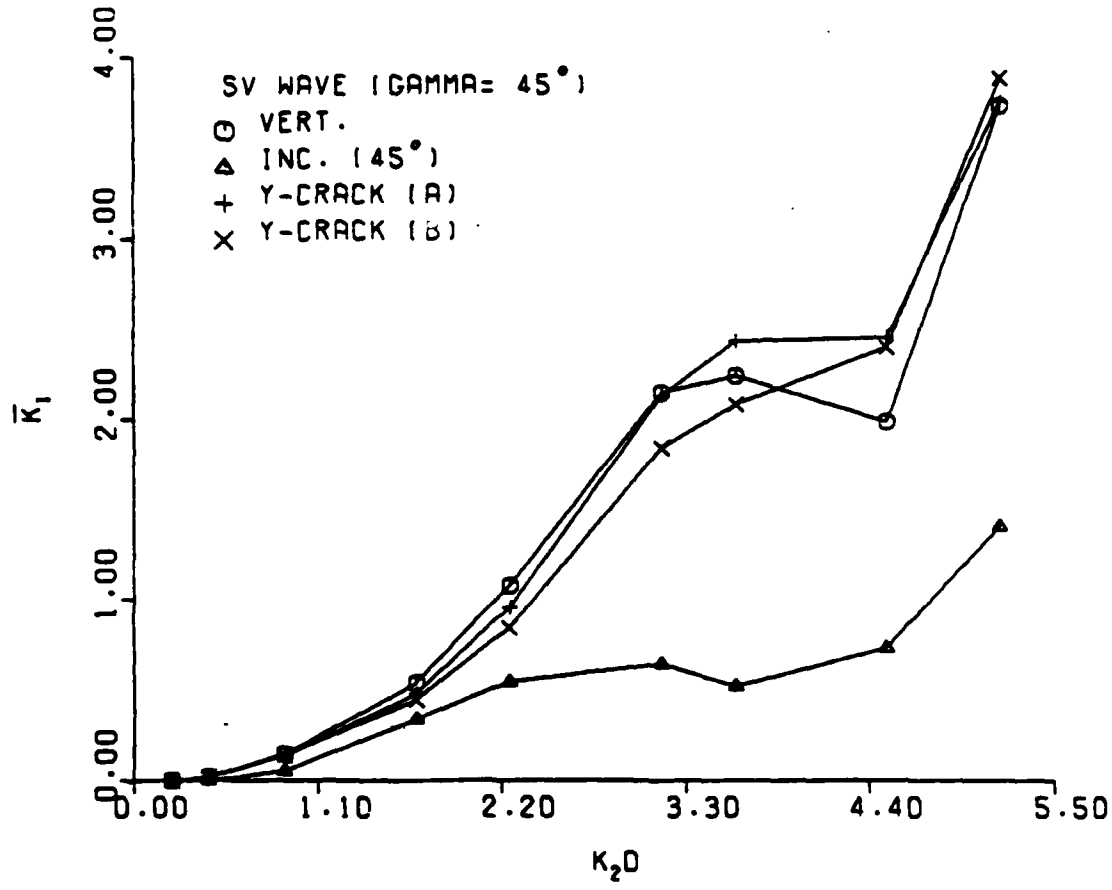
SV WAVE (GAMMA= 45°)
VERT.
INC. (45°)
Y-CRACK (A)
Y-CRACK (B)
$\bar{K}_I$
0.00
1.00
2.00
3.00
4.00
0.00
1.10
2.20
3.30
4.40
5.50
K_2D

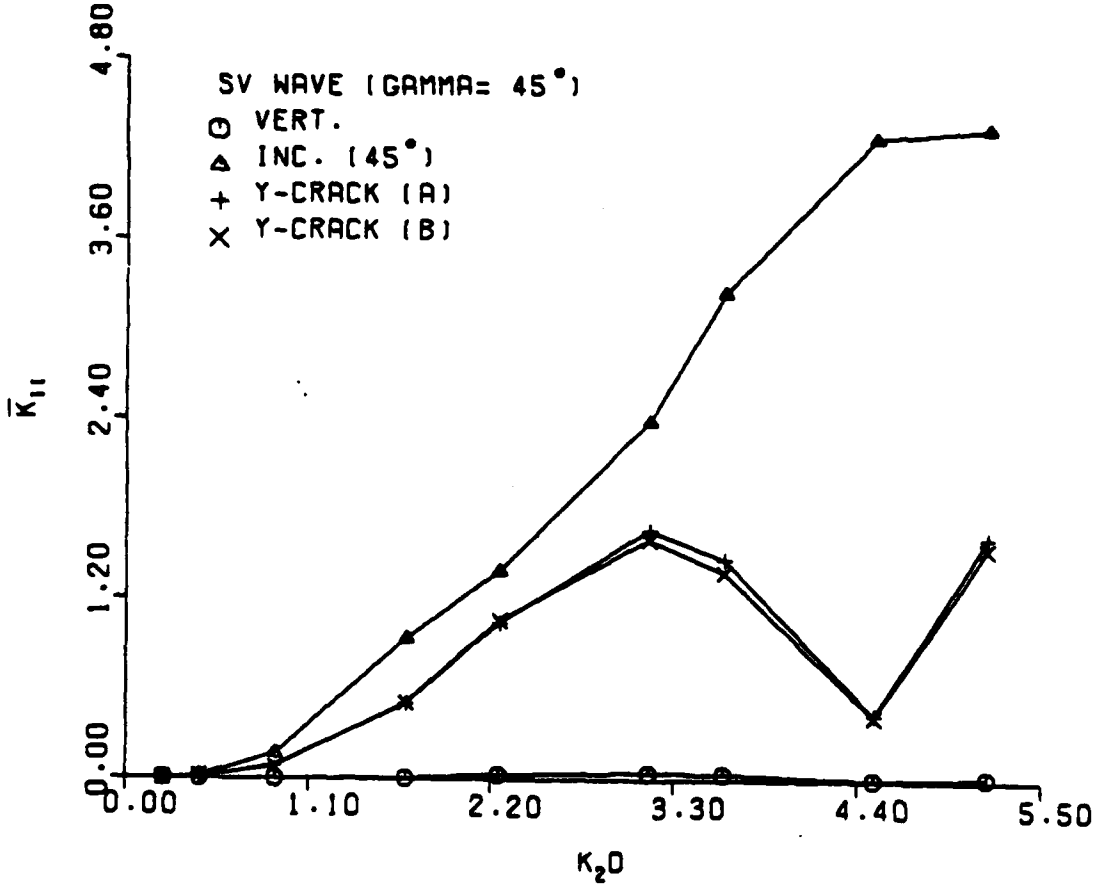
SV WAVE (GAMMA= 45°)
VERT.
INC. (45°)
Y-CRACK (A)
Y-CRACK (B)
$\bar{K}_{II}$
0.00
1.20
2.40
3.60
4.80
0.00
1.10
2.20
3.30
4.40
5.50
K_2D

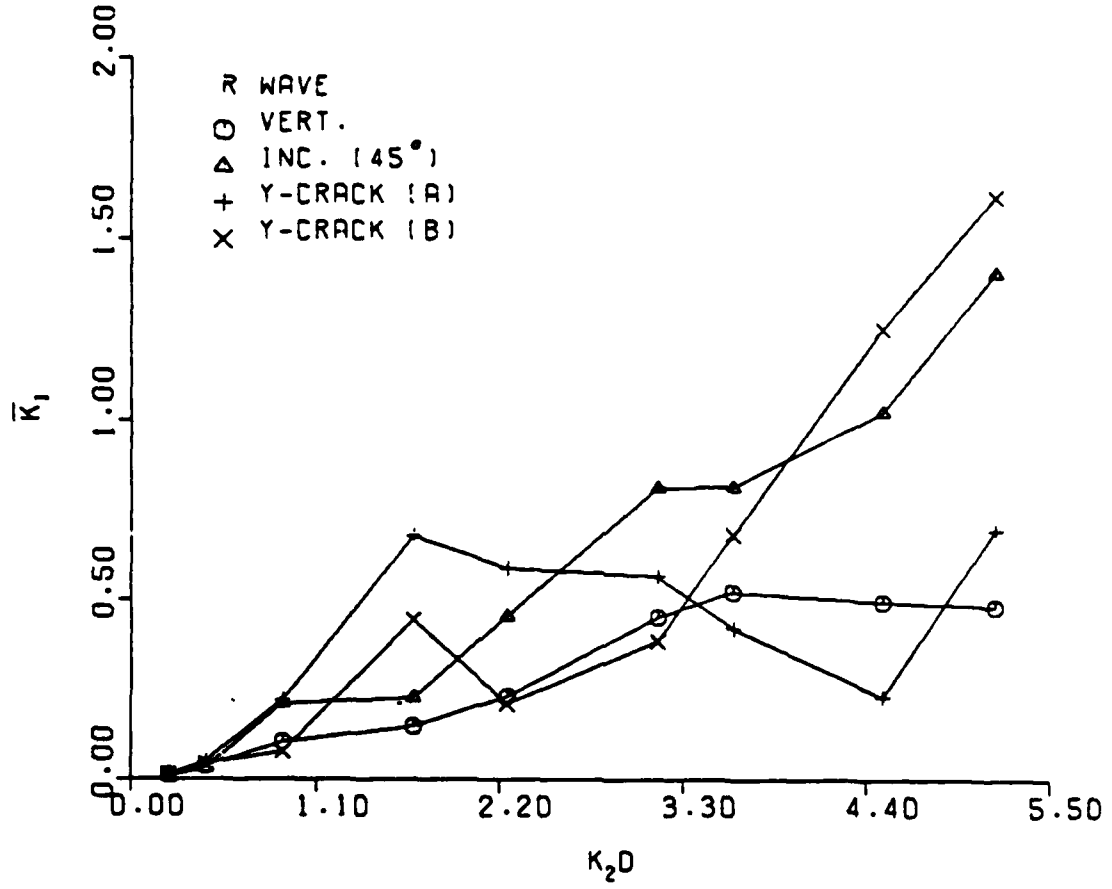
R WAVE
VERT.
INC. (45°)
Y-CRACK (A)
Y-CRACK (B)
$\bar{K}_I$
0.00
0.50
1.00
1.50
2.00
0.00
1.10
2.20
3.30
4.40
5.50
K_2D

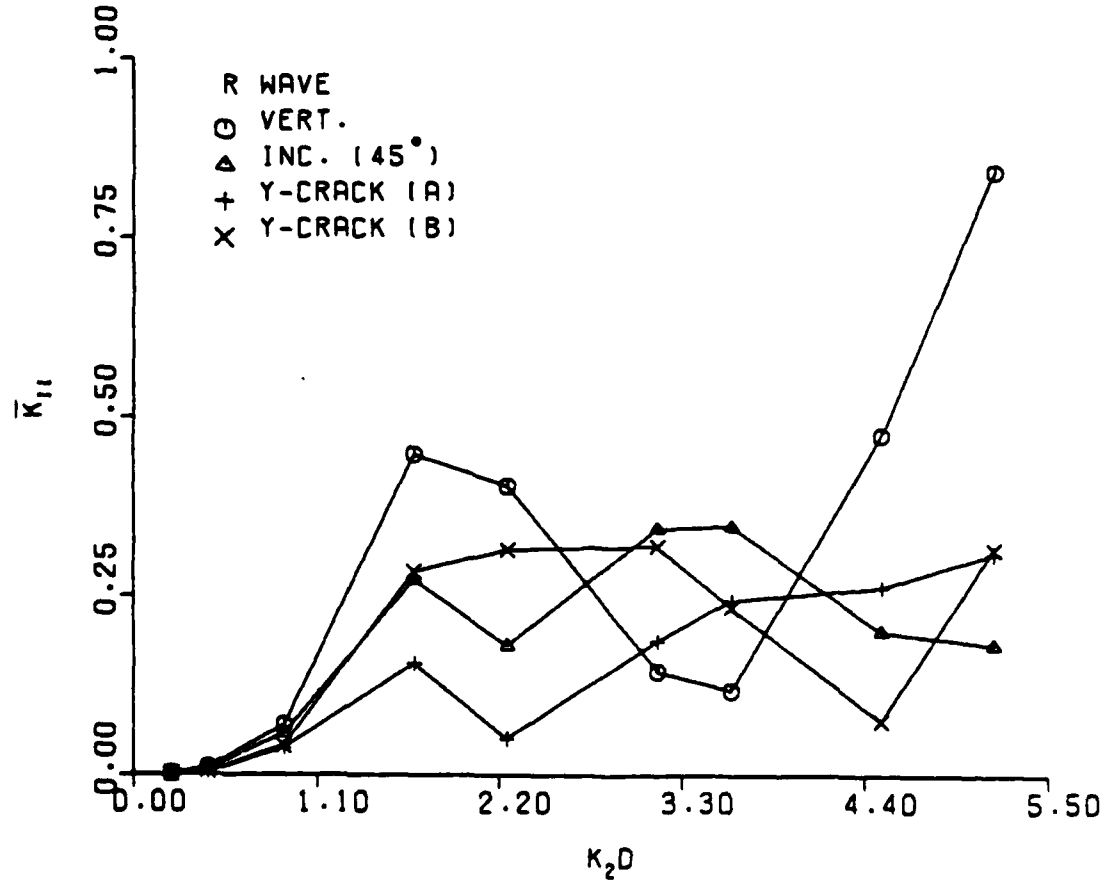
R WAVE
VERT.
INC. (45°)
Y-CRACK (A)
Y-CRACK (B)
$\bar{K}_{II}$
0.00
0.25
0.50
0.75
1.00
0.00
1.10
2.20
3.30
4.40
5.50
K_2D

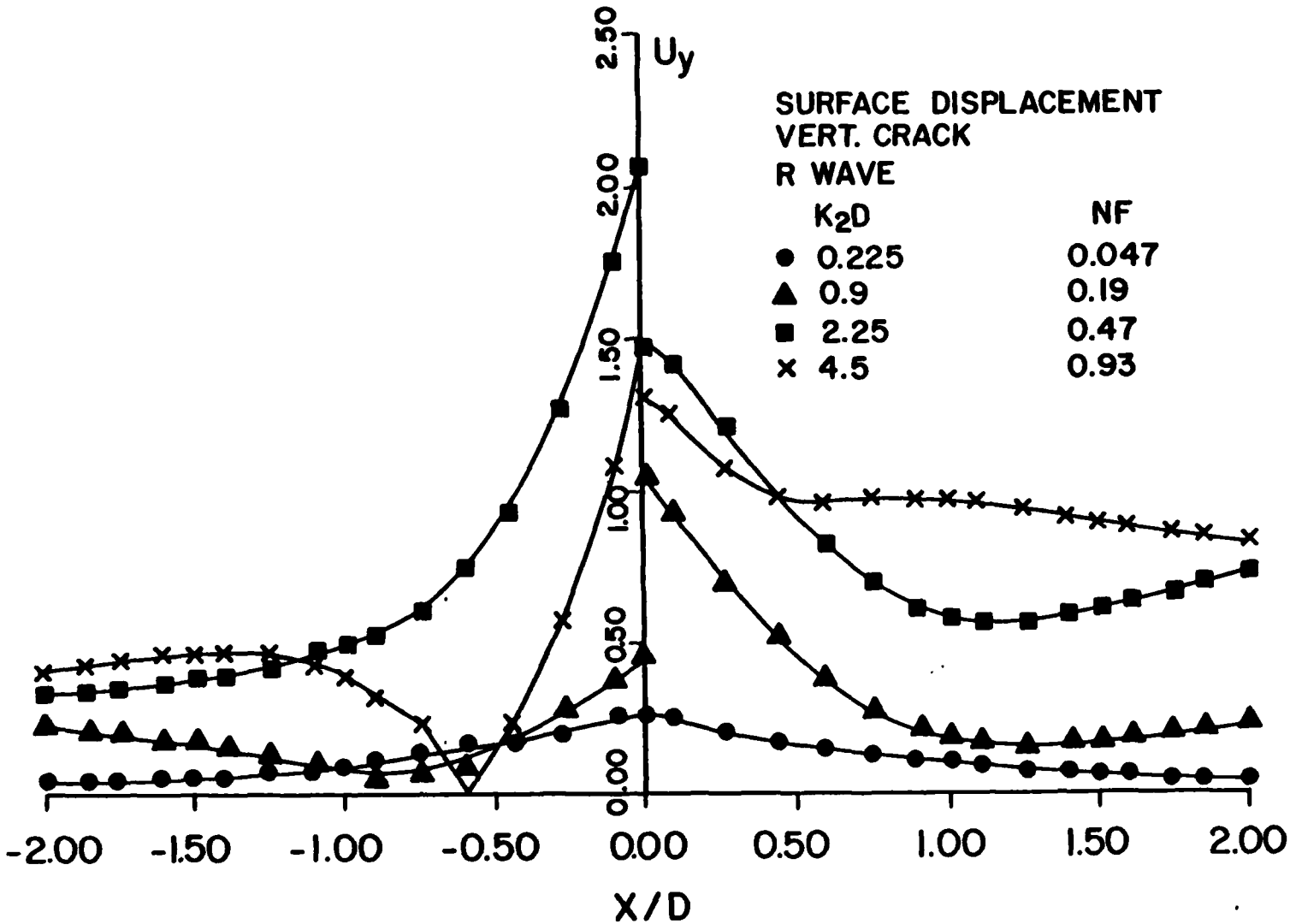
SURFACE DISPLACEMENT
VERT. CRACK
R WAVE
K2D
NF
0.225
0.047
0.9
0.19
2.25
0.47
4.5
0.93
Uy
2.50
2.00
1.50
1.00
0.50
0.00
-2.00
-1.50
-1.00
-0.50
0.00
0.50
1.00
1.50
2.00
X/D

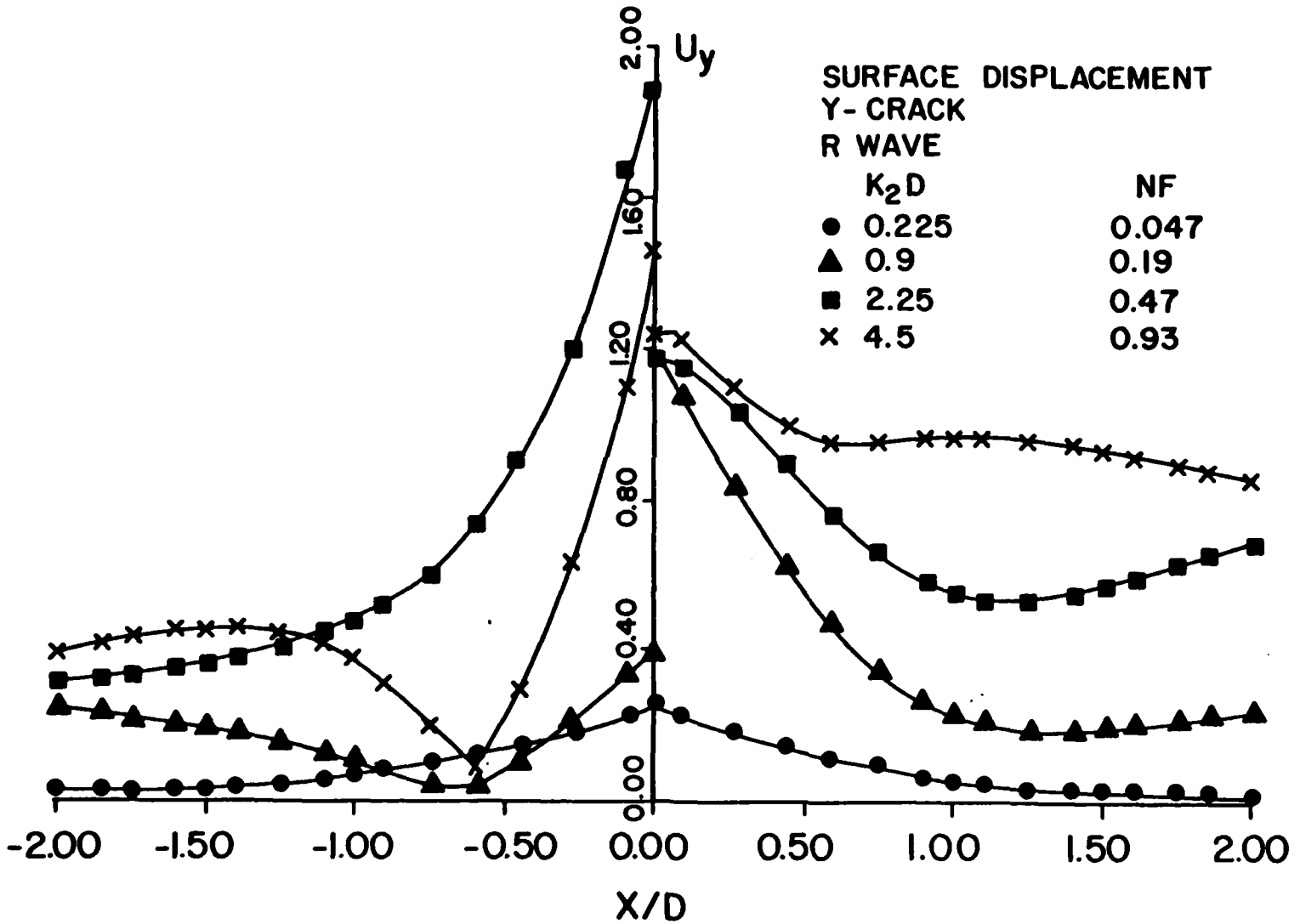
SURFACE DISPLACEMENT
Y- CRACK
R WAVE
K_2D NF
0.225 0.047
0.9 0.19
2.25 0.47
4.5 0.93
U_y
2.00
1.60
1.20
0.80
0.40
0.00
-2.00 -1.50 -1.00 -0.50 0.00 0.50 1.00 1.50 2.00
X/D

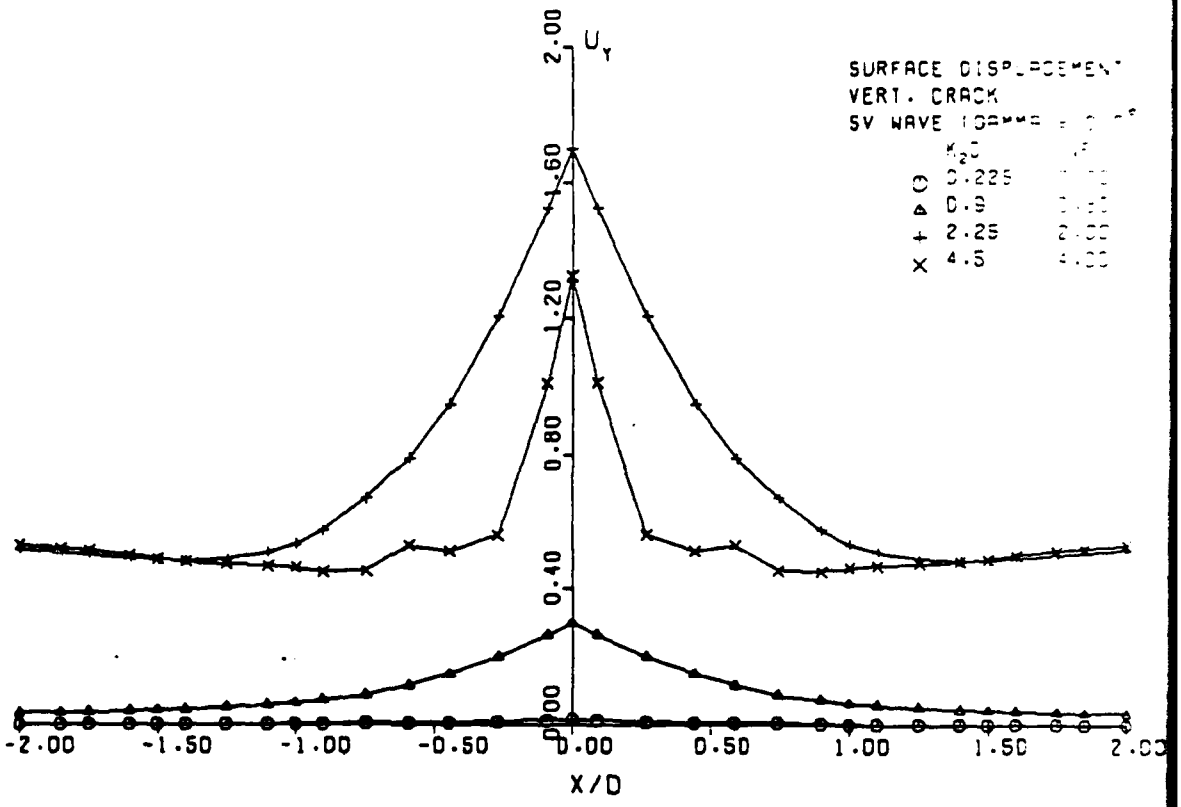
SURFACE DISPLACEMENT
VERT. CRACK
SV WAVE (GAMMA = 0.0°)
K_2D NF
○ 0.225
△ 0.9
+ 2.25
× 4.5
U_Y
2.00
1.60
1.20
0.80
0.40
0.00
-2.00
-1.50
-1.00
-0.50
0.00
0.50
1.00
1.50
2.00
X/D

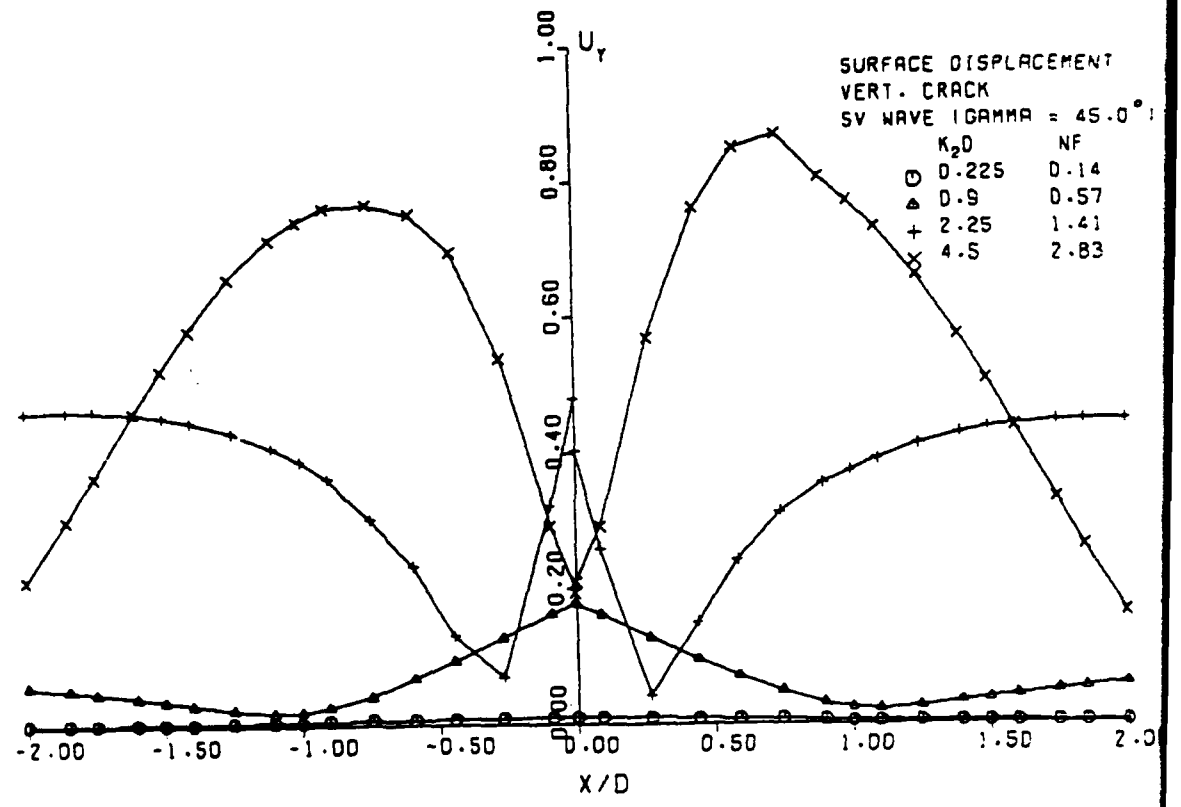
SURFACE DISPLACEMENT
VERT. CRACK
SV WAVE (GAMMA = 45.0°)
K_2D NF
○ 0.225 0.14
△ 0.9 0.57
+ 2.25 1.41
× 4.5 2.83
U_Y
1.00
0.80
0.60
0.40
0.20
0.00
-2.00
-1.50
-1.00
-0.50
0.00
0.50
1.00
1.50
2.00
X/D

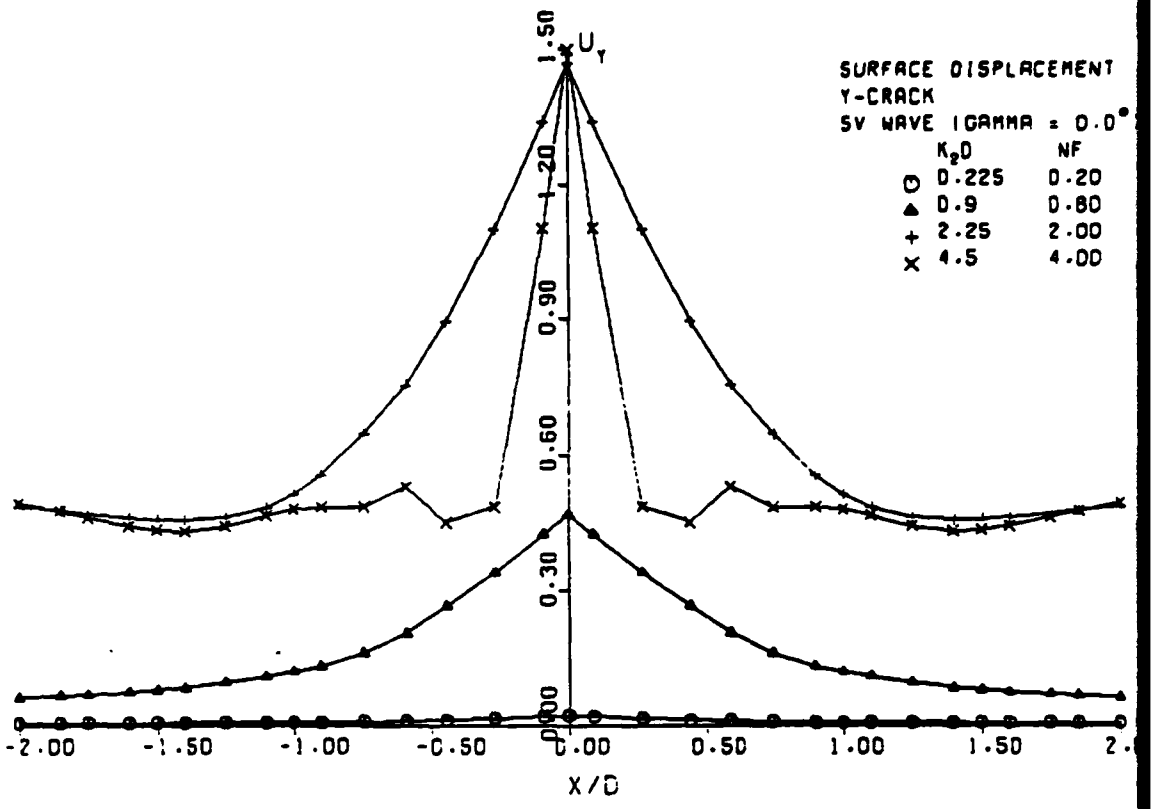
SURFACE DISPLACEMENT
Y-CRACK
SV WAVE (GAMMA = 0.0°
K2D NF
0.225 0.20
0.9 0.80
2.25 2.00
4.5 4.00
Uy
1.50
1.20
0.90
0.60
0.30
0.00
-2.00
-1.50
-1.00
-0.50
0.00
0.50
1.00
1.50
X/D

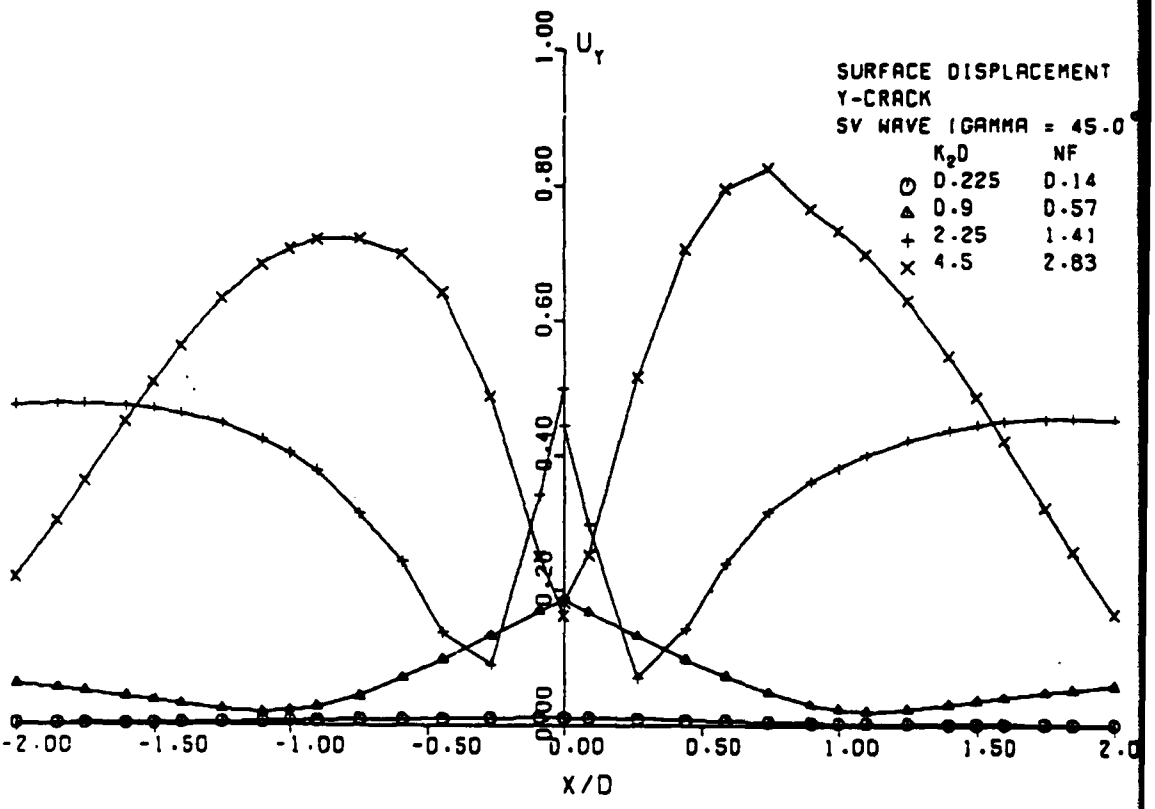
SURFACE DISPLACEMENT
Y-CRACK
SV WAVE (GAMMA = 45.0°
K2D NF
0.225 0.14
0.9 0.57
2.25 1.41
4.5 2.83
Uy
1.00
0.80
0.60
0.40
0.20
0.00
-2.00
-1.50
-1.00
-0.50
0.00
0.50
1.00
1.50
X/D

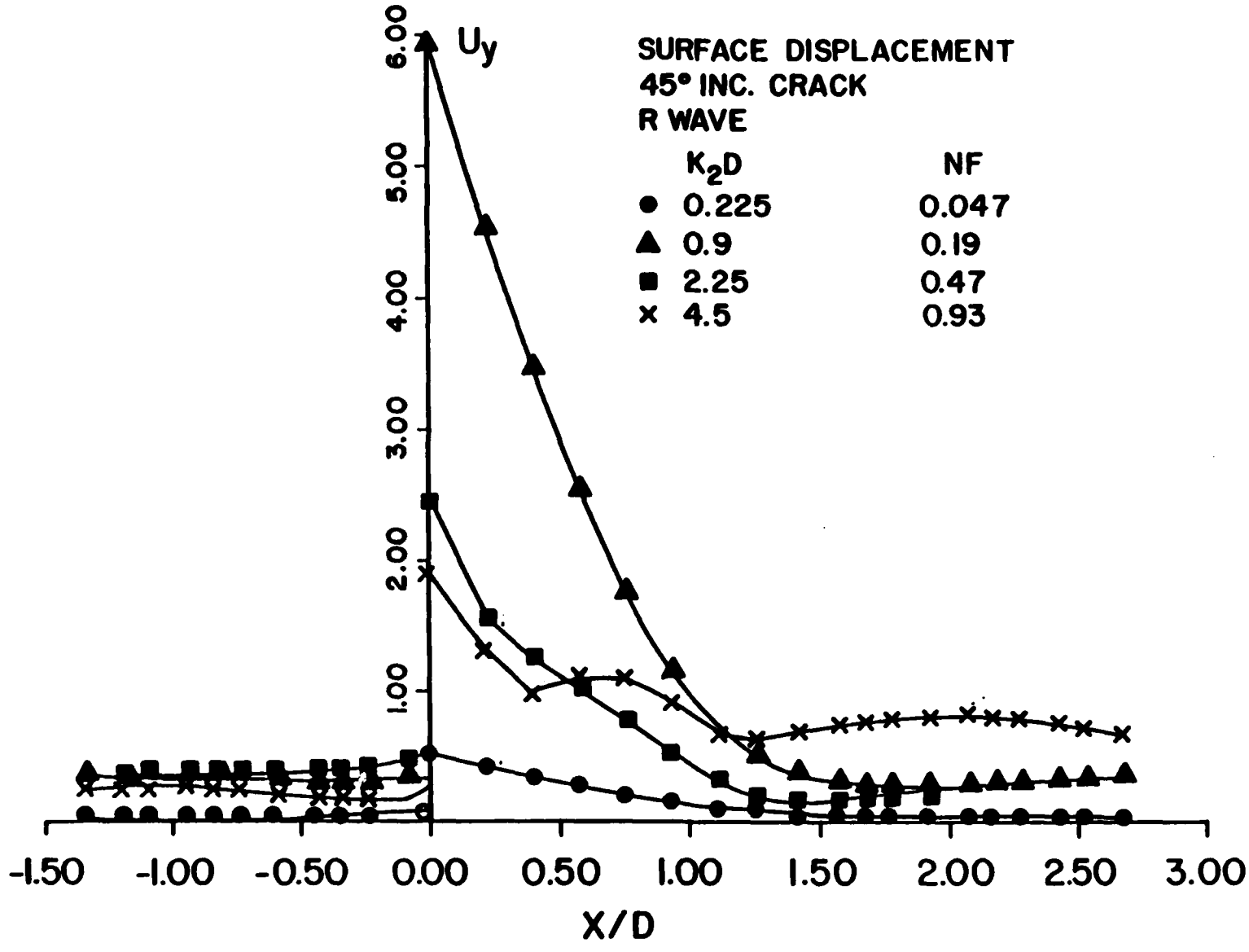
SURFACE DISPLACEMENT
45° INC. CRACK
R WAVE
K_2D NF
0.225 0.047
0.9 0.19
2.25 0.47
4.5 0.93
U_y
6.00
5.00
4.00
3.00
2.00
1.00
-1.50
-1.00
-0.50
0.00
0.50
1.00
1.50
2.00
2.50
3.00
X/D

END

10-86

DTIC